

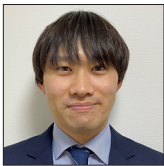


Original Research Imaging Science

Integration of dual-energy computed tomography and radiomics to improve noninvasive assessment of liver fibrosis: A retrospective study

Takayuki Miyachi¹, Shintaro Ichikawa¹, Tatsunori Kobayashi¹, Akihiro Osugi¹, Ren Suzuki¹, Masatoshi Kakuya¹, Satoshi Funayama¹, Yukichi Tanahashi¹, Kumi Ozaki¹, Satoshi Goshima¹

¹Department of Radiology, Hamamatsu University School of Medicine, Hamamatsu, Japan.



***Corresponding author:**

Takayuki Miyachi,
Department of Radiology,
Hamamatsu University School
of Medicine, Hamamatsu,
Japan.

miyachi.takayuki117@gmail.com

Received: 22 October 2025
Accepted: 10 January 2026
Published: 23 February 2026

DOI
10.25259/JCIS_255_2025

Quick Response Code:



ABSTRACT

Objectives: Few studies have used radiomics analysis to virtual monochromatic images (VMI) and material density images (MDI) for the assessment of liver fibrosis. Therefore, this retrospective study aimed to investigate whether integrating dual-energy computed tomography (CT) with radiomics analysis can predict Fibrosis-4 (FIB-4) index risk groups.

Material and Methods: A total of 137 patients were classified on the basis of the FIB-4 index: 40 as low-risk (FIB-4 index <1.3), 57 as intermediate-risk (1.3 ≤ FIB-4 index <2.67), and 40 as high-risk (FIB-4 index ≥2.67) for liver fibrosis. VMIs (70-keV and 40-keV images) and MDI (iodine-water images) were generated from the equilibrium-phase dual-energy CT data, and radiomic features were extracted from the same liver segmentation to develop models for distinguishing between FIB-4 risk groups.

Results: Distinguishing between low-risk and high-risk groups yielded mean area under the curve (AUC) values (95% confidence intervals) of 0.69 (0.57–0.80) for the 70-keV images, 0.77 (0.67–0.88) for the 40-keV images, and 0.77 (0.66–0.87) for the iodine-water images, with statistically significant differences between the 70-keV images and the 40-keV ($P = 0.01$) and iodine-water images ($P = 0.04$). To distinguish between the low-risk and intermediate-risk groups, all image types showed similar AUC values ranging from 0.64 to 0.66, with no significant differences. For distinguishing intermediate-risk and high-risk groups, the 40-keV and iodine-water images showed a trend toward higher AUC values than the 70-keV images; however, no statistically significant differences were observed.

Conclusion: This study demonstrates the feasibility of combining dual-energy CT with radiomics for noninvasive liver fibrosis risk stratification using the FIB-4 index.

Keywords: Dual-energy computed tomography, Liver fibrosis, Radiomics

INTRODUCTION

Diffuse liver disease is highly prevalent worldwide. Liver disease accounts for approximately 2 million deaths annually, representing 4% of all global mortality.^[1] Liver fibrosis is characterized by the progression of chronic liver disease and serves as a critical factor in determining liver disease outcomes and risks.^[2,3]

Liver biopsy is currently considered the gold standard for assessing liver fibrosis. However, it has notable limitations, including its invasive nature, potential sampling inaccuracies, and observer dependency.^[4]

This is an open-access article distributed under the terms of the Creative Commons Attribution-Non Commercial-Share Alike 4.0 License, which allows others to remix, transform, and build upon the work non-commercially, as long as the author is credited and the new creations are licensed under the identical terms.

©2026 Published by Scientific Scholar on behalf of Journal of Clinical Imaging Science

The fibrosis index based on four factors (Fibrosis-4 [FIB-4] index) is a simple, inexpensive, and noninvasive method that correlates with the stage of fibrosis in patients. Although the FIB-4 index has several limitations, it is useful for assessing the stage of liver fibrosis in patients with chronic liver diseases.^[5]

Various noninvasive imaging techniques, such as ultrasonography (US)^[6,7] and magnetic resonance (MR) imaging,^[6,8,9] have been developed. However, these imaging methods have drawbacks; US can be influenced by the operator's skill level,^[7] whereas MR may have limited accessibility.^[8]

Computed tomography (CT) has emerged as a noninvasive imaging modality for assessing liver fibrosis.^[10,11] It offers several advantages, including easy accessibility, reduced operator dependence, and the ability to rapidly scan images of the entire liver. Recently, dual-energy CT, an innovative technology, has become available for clinical use. Dual-energy CT scans an object using two different energy levels of X-rays to provide additional information, for example, virtual monochromatic images (VMI) and material density images (MDI). VMI and MDI can enhance contrast and iodine signals on contrast-enhanced CT.^[12,13]

Advances in image processing, particularly in radiomics analysis, have further expanded the potential of CT-based diagnostics. Radiomics analysis mathematically quantifies image features and offers the potential to extract features that are not always clear through visual evaluations.^[14,15]

As liver fibrosis primarily affects the extracellular extravascular space,^[3] where iodine contrast material distributes, contrast-enhanced CT is a suitable modality for evaluating liver fibrosis. Although combining VMI and MDI with radiomics analysis may improve their potential for evaluating liver fibrosis, their practical utility and effectiveness remain poorly understood. To the best of our knowledge, few studies have used radiomics analysis of VMI and MDI for this purpose.

Here, we aimed to investigate whether the integration of dual-energy CT imaging with radiomics analysis enables risk stratification based on the FIB-4 index. This exploratory, hypothesis-generating investigation was designed to assess the feasibility of this approach.

MATERIAL AND METHODS

Study design and patients

This single-center retrospective study was approved by our Institutional Research Ethics Committee (approval number: 22-169), which waived the requirement for informed consent. All patients underwent clinically indicated dual-energy contrast-enhanced abdominal CT between March

and September 2022. The inclusion criteria were as follows: (1) Patients aged 18 years or older, (2) availability of equilibrium-phase images (3 min after contrast material injection), and (3) serum markers obtained within 3 months before or after the CT examination. Serum markers, including aspartate aminotransferase (AST), alanine transaminase (ALT), and platelet counts, were used to calculate the FIB-4 index.

FIB-4 index

The FIB-4 index was calculated using the following formula: Age [years] \times AST level [U/L]/(platelet count [10^9 /L] \times ALT level [U/L]^{1/2}). The data were divided into three groups according to risk. A FIB-4 index <1.3 was categorized as low-risk, whereas a FIB-4 index ≥ 2.67 was categorized as high-risk for liver fibrosis.^[5,16] A FIB-4 index between the low-risk and high-risk groups was categorized as intermediate-risk.

CT acquisition techniques

CT examinations were performed using a single-source, dual-energy CT scanner with fast kV switching (Revolution CT; GE Healthcare, Milwaukee, WI, USA). Iodine contrast material (240–370 mgI/mL) was injected at a dose of 600 mgI/kg of body weight using a power injector over 30–40 s. A dynamic study including pre-contrast, arterial, portal venous, and equilibrium-phase images was performed, and only the equilibrium phase was used for analysis. Equilibrium-phase images of dual-energy were scanned 3 min after contrast material injection using the following scanning parameters: tube voltage, 80/140 kVp; tube current, 350–900/200–515 mA; gantry rotation speed, 0.5 or 0.8 s; pitch, 0.992; total collimation width, 80 mm; matrix, 512 \times 512; field of view, 320–440 mm; slice thickness, 0.625 mm; and reconstruction algorithm, deep learning image reconstruction (TrueFidelity) medium. The tube current was controlled by the noise index (14.8 or 15.5 for 2.5-mm slice images).

Radiomics

Projection data from the equilibrium-phase images were sent to a workstation (AW Server 3.2 Ext.4.0; GE Healthcare, Milwaukee, WI, USA) and post-processed using dual-energy software (Volume Viewer 16.0 Ext.2; GE Healthcare, Milwaukee, WI, USA) to generate 70-keV and 40-keV images of VMI and iodine-water images of MDI. One reader (a medical physicist with 5 years of experience) defined the regions of interest (ROIs) for the three-dimensional (3D) liver volume of all patients. Automatic 3D entire liver volume segmentation was performed by Hepatic VCAR software on this workstation to improve the reproducibility of the ROIs. These images and ROIs were sent to the 3D Slicer

software.^[17] The ROIs were further edited to exclude lesions, the main portal vein, and other major veins, while correcting any obviously inappropriate areas, including metal artifacts. Then, the ROIs were shrunk by 3 mm to eliminate the partial volume effects at the liver margin. Figure 1 shows an example of the workflow used for ROI delineation. To explore the stability of each feature, 30 patients were randomly selected, and the intraclass correlation coefficient (ICC) was quantified according to a previous study^[11] and guidelines.^[18] Another reader (a radiation technologist with 19 years of experience) independently defined the 3D ROIs to evaluate interobserver reproducibility. The radiomic features of each image with the same 3D ROIs were calculated using the SlicerRadiomics extension (version 3.1.0) of the 3D Slicer software. The voxel spacing was standardized to a size of 1 mm × 1 mm × 1 mm, and the voxel intensity values were discretized with a bin width of 1 HU. The radiomic features included 16 first-order features, 24 gray-level co-occurrence matrix features, 16 gray-level run length matrix features, 16 gray-level size zone matrix features, five neighboring gray tone difference matrix features, and 14 gray-level dependence matrix features. Features confounded by the shape or volume of the ROIs were not included because lesions and artifact areas were excluded.

Model establishment and statistical analysis

Models for distinguishing between each pair of FIB-4 index risk groups in each of the datasets of 70-keV, 40-keV, and iodine-water images were created using a support vector machine (SVM) classifier. Preliminary filtering steps

were applied to remove unreliable features, features with minimal association with the FIB-4 index, and to mitigate multicollinearity. First, features with ICCs ≥ 0.80 were kept for further analysis. Second, Mann–Whitney U-tests were performed between each pair of FIB-4 index risk groups, and features with $P > 0.10$ between all groups were removed. Third, Spearman correlation tests were performed for each dataset, and among features with correlation coefficients > 0.90 , only one feature was retained while the others were removed. Following these preliminary filtering steps, final feature selection and model establishment were performed using an SVM classifier within a cross-validation framework. Specifically, a stratified four-fold cross-validation was used for model evaluation, with feature selection conducted independently within each training fold using an internal cross-validation procedure. To reduce the risk of overfitting, no more than three features were selected for model establishment, considering that the minimum number of samples in a training fold was 30. Model performance was evaluated using receiver operating characteristic (ROC) curves and area under the curve (AUC) metrics. We generated ROC curves for each fold as well as the mean ROC curves across all folds for each condition. To assess the statistical significance of our results, we implemented DeLong tests to compare the AUCs, which accounted for the correlated nature of the ROC curves. We also calculated 95% confidence intervals (CI) for the AUCs using the DeLong method. All model establishment and statistical analyses were performed using an in-house Python script in a Jupyter Notebook (version 7.0.8) on Anaconda Navigator (version 2.6.2; Anaconda Inc., Austin, TX, USA).

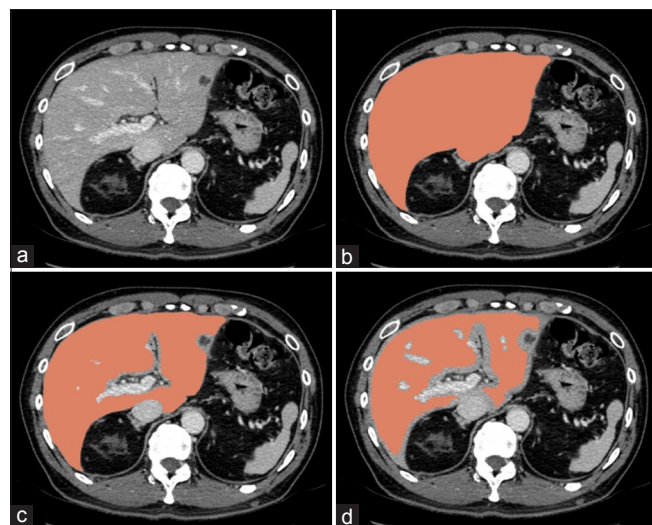


Figure 1: Example of delineation of regions of interest (ROIs). (a) computed tomography images. (b) ROIs (the red region) of the entire three-dimensional liver volume. (c) ROIs with liver parenchyma excluding the lesions, main portal vein, and other structures. (d) Final ROIs after 3 mm of shrinkage.

RESULTS

Study population

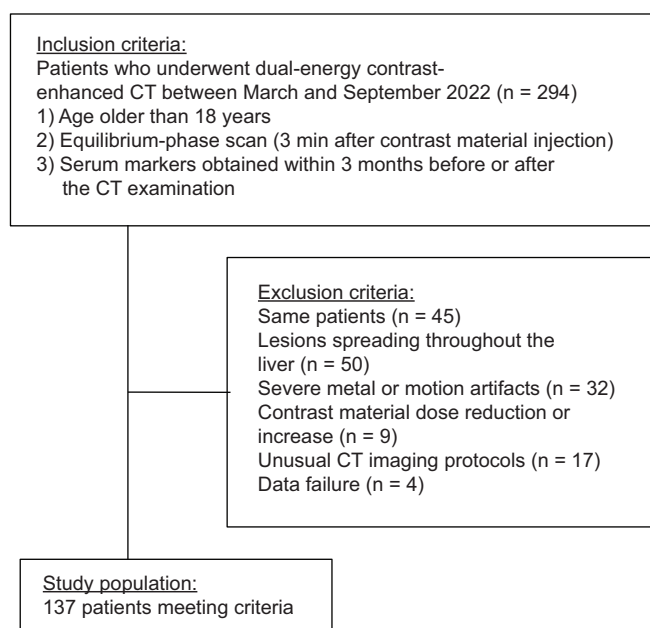
In total, 294 consecutive patients who met study criteria were screened. The reasons for exclusion were as follows: duplicate scans of the same patient ($n = 45$; only the most recent scan was included), lesions spreading throughout the liver ($n = 50$), severe metal or motion artifacts ($n = 32$), dose reduction or increase in contrast material ($n = 9$), unusual CT imaging protocols ($n = 17$), and data failure ($n = 4$). Finally, 137 patients (104 men and 33 women) were included in this study [Figure 2].

The risk groups were classified according to the FIB-4 index as follows: low-risk, 40 patients; intermediate-risk, 57 patients; and high-risk, 40 patients. The clinical features are summarized in Table 1. No significant differences were found among the three groups in terms of sex. Body weight was lower in the intermediate-risk group than in the other groups; however, no significant differences were

Table 1: Demographic data of the patients.

	FIB-4 index			P-values		
	Low	Intermediate	High	Low-high	Low-intermediate	Intermediate-high
Number of patients	40	57	40	–	–	–
Sex, male/female	31/9	39/18	34/6	>0.99	>0.99	0.28
Body weight (kg)	62.6±10.9	55.5±9.8	60.3±10.3	0.48	0.001	0.07
Body mass index (kg/m ²)	23.0±3.4	21.7±3.4	22.8±3.4	>0.99	0.09	0.07
FIB-4 index	0.98±0.25	1.92±0.38	5.57±3.35	<0.001	<0.001	<0.001
Age (years)	62.5±13.1	73.9±9.4	71.9±9.5	0.003	<0.001	0.57
ALT (U/L)	31.4±40.0	24.9±26.1	60.4±128.3	0.38	0.27	0.01
AST (U/L)	22.2±11.9	26.2±14.0	94.5±186.9	<0.001	0.08	<0.001
Platelet count (10 ⁴ /μL)	28.4±6.8	22.3±7.2	14.3±5.9	<0.001	<0.001	<0.001

FIB-4: Fibrosis-4, ALT: Alanine transaminase, AST: Aspartate aminotransferase. Categorical variables are presented as the number of cases. Continuous variables are presented as mean±standard deviation. $P<0.05$ after Bonferroni correction was considered significant.

**Figure 2:** Study flowchart. CT: Computed tomography.

observed between the low-risk and high-risk groups. Significant differences were observed among the three groups for the FIB-4 index and most of the factors used in its calculation. Of the 137 patients included in this study, 47 had the following chronic liver diseases: hepatitis B infection, $n = 7$; hepatitis C infection, $n = 11$; coinfection with hepatitis B and C, $n = 3$; alcoholic hepatitis, $n = 2$; primary biliary cholangitis, $n = 2$; autoimmune hepatitis, $n = 3$; and other causes, $n = 19$. Of these, 23 patients had liver cirrhosis. The details are summarized in Table 2.

Feature selection

Among the 91 radiomic features, ICC analysis retained 57, 56, and 51 features for the 70-keV, 40-keV, and iodine-

Table 2: Causes of chronic liver disease.

Etiology	FIB-4 index		
	Low	Intermediate	High
No known chronic liver disease	33	42	15
Hepatitis B infection	1 (1)	2	4 (2)
Hepatitis C infection	2 (1)	3 (3)	6 (4)
Hepatitis B and C infection	0	3 (1)	0
Alcoholic hepatitis	0	0	2 (1)
Primary biliary cholangitis	1 (1)	0	1 (1)
Autoimmune hepatitis	0	2	1
Others	3 (2)	5 (1)	11 (5)

FIB-4: Fibrosis-4. Categorical variables are presented as the number of cases. The numbers in parentheses indicate the number of patients with cirrhosis among these cases.

water images, respectively. Subsequently, the Mann-Whitney U-test results retained 51, 50, and 47 features for the 70-keV, 40-keV, and iodine-water images, respectively. Finally, Spearman correlation test results indicated 5, 5, and 7 features for the 70-keV, 40-keV, and iodine-water images, respectively.

Model performance

The ROC curves for each condition are shown in Figure 3. The ROC analysis for distinguishing between low-risk and high-risk groups yielded mean AUC values (95% CI) of 0.69 (0.57–0.80), 0.77 (0.67–0.88), and 0.77 (0.66–0.87) for the 70-keV, 40-keV, and iodine-water images, respectively [Figure 3a-c]. A statistically significant difference was observed between the AUC values of the 70-keV and 40-keV images ($P = 0.01$) and between the 70-keV and iodine-water images ($P = 0.04$). For distinguishing low-risk and intermediate-risk groups, all image types showed comparable

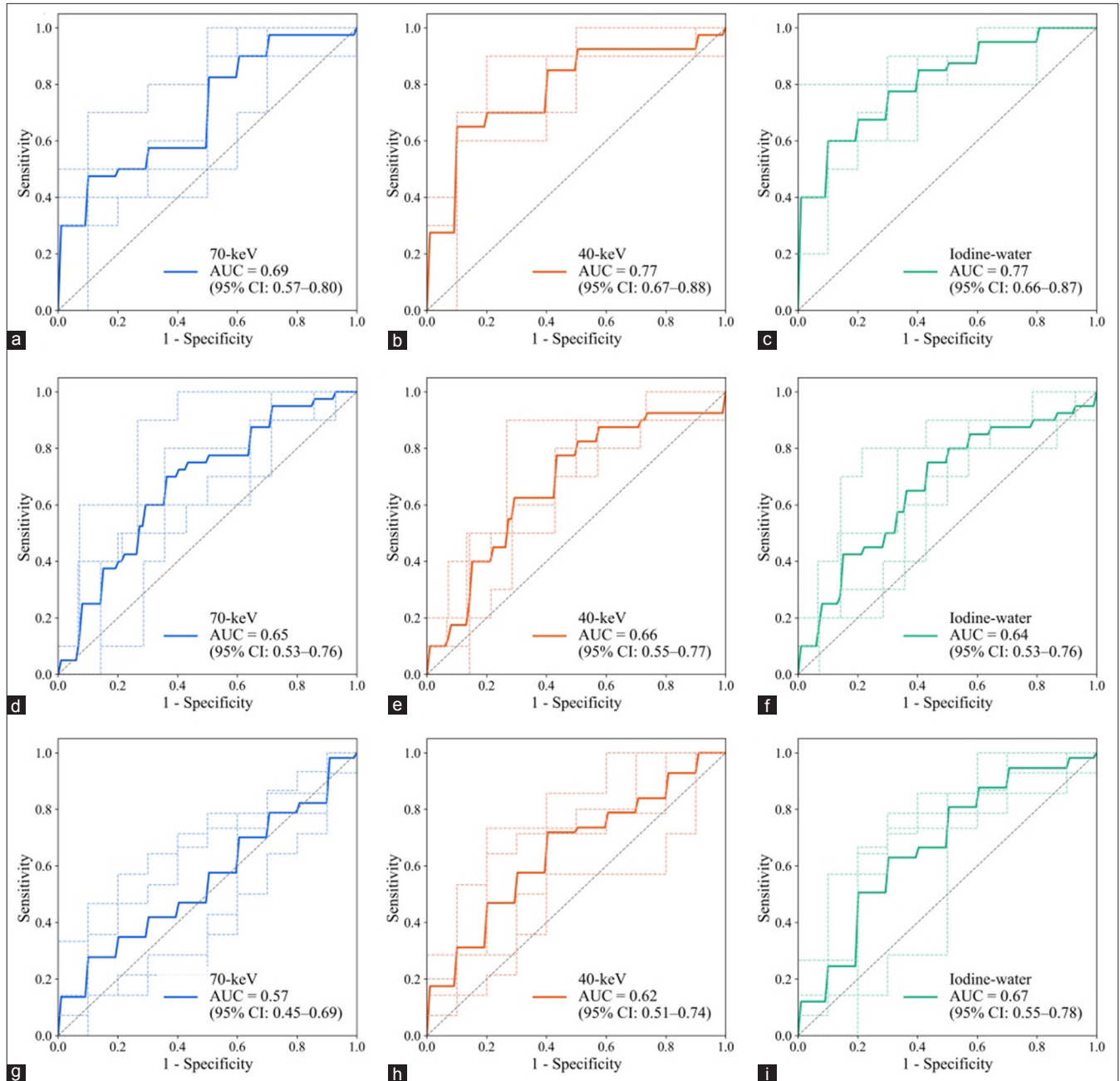


Figure 3: ROC curves for each pair of FIB-4 index groups. (a-c) ROC curves for low-risk and high-risk groups; (d-f) low-risk and intermediate-risk groups; (g-i) intermediate-risk and high-risk groups. (a, d, g) 70-keV, (b, e, h) 40-keV, (c, f, i) iodine-water images. Solid lines indicate mean ROC curves; dotted lines indicate individual fold ROC curves. ROC: Receiver operating characteristic, FIB-4: Fibrosis-4, AUC: Area under the curve, 95% CI: 95% confidence interval.

mean AUC values (95% CI), ranging from 0.64 (0.53–0.76) to 0.66 (0.55–0.77), with no statistically significant differences [Figure 3d-f]. ROC analysis for distinguishing intermediate-risk and high-risk groups yielded mean AUC values (95% CI) of 0.57 (0.45–0.69), 0.62 (0.51–0.74), and 0.67 (0.55–0.78) for the 70-keV, 40-keV, and iodine-water images, respectively [Figure 3g-i]. However, no statistically significant differences were observed between the AUC values of the 70-keV and

40-keV images ($P = 0.20$) or between the 70-keV and iodine-water images ($P = 0.07$).

DISCUSSION

The results of this study indicate that models based on radiomic features extracted from VMI or MDI using dual-energy CT in the equilibrium phase can effectively stratify

FIB-4 index risk groups. Few studies have evaluated liver fibrosis by combining VMI or MDI created using dual-energy CT with radiomics. Here, the AUC values of VMI (40-keV) and MDI (iodine-water) were larger than those of 70-keV images, which are equivalent to single-energy CT images;^[19] additionally, significant differences were observed between the low-risk and high-risk groups. These results suggest that dual-energy CT may improve prediction of FIB-4 index risk groups compared with single-energy CT.

For distinguishing low-risk and high-risk groups, the mean AUC value of the 70-keV images was 0.69, whereas the mean AUC values of the 40-keV and iodine-water images were both 0.77. An improvement of approximately 0.1 in AUC values is generally interpreted as reflecting enhanced clinical interpretability of diagnostic performance.^[20] Dual-energy CT can be performed using a workflow similar to that of single-energy CT without requiring an additional complex workflow, while potentially improving diagnostic performance. Therefore, this approach may represent a useful strategy for risk enrichment in routine clinical practice using dual-energy CT.

Lower-keV VMI with dual-energy CT emphasize iodine contrast enhancement.^[21] Moreover, a previous study has reported that the stage of liver fibrosis can be evaluated noninvasively on the basis of iodine concentration in iodine-water images of MDI.^[22] The enhancement of contrast in imaging through VMI and MDI may have emphasized the contrast material present in the extracellular space of the liver, potentially improving the accuracy of evaluating risk stratification based on the FIB-4 index. Radiomics analysis is expected to improve the accuracy of diagnosis, prognostic evaluation, and prediction of treatment responses.^[15] Radiomics analysis of contrast-enhanced CT images in single-energy CT has been reported to significantly improve the diagnostic ability of liver fibrosis.^[11] The results of this study indicate that radiomics analysis of contrast-enhanced dual-energy CT images can, similarly to single-energy CT, be used for evaluating risk stratification based on the FIB-4 index. Furthermore, our findings suggest that the combination of dual-energy CT and radiomics may show higher accuracy than the combination of single-energy CT and radiomics in evaluating risk stratification based on the FIB-4 index.

In the present study, 3D ROIs were placed on the liver such that the analysis volume encompassed the entire liver parenchyma. The results suggest that the FIB-4 index can be predicted from the entire liver parenchyma without the need to select a specific region. At present, automatic organ segmentation technology is being developed to make it possible to automatically segment the liver.^[23] In the future, it will be possible to evaluate the localization of fibrosis in automatically segmented livers.

The hepatic extracellular volume, assessed using the equilibrium phase, correlates with the degree of fibrosis.^[24]

The normalized iodine concentration in the liver on the 5-min delayed dual-energy CT also showed a strong correlation with the histological stage of liver fibrosis.^[25] The fractional extracellular space assessed on dual-energy CT at the equilibrium phases with 3-min and 10-min delayed phases showed substantial similarity.^[26] In the present study, it was possible to evaluate the FIB-4 index using 3-min delayed equilibrium-phase images. However, further comparative studies are needed to clarify differences between the 3-min delayed phase and longer delayed phases.

This study has some limitations. First, the FIB-4 index was used for fibrosis risk stratification, and liver biopsy or elastography was not used as a reference standard. The use of the FIB-4 index as a surrogate marker has strengths and limitations. The FIB-4 index is a simple, noninvasive, and clinically validated index; however, it does not provide a direct measure of liver stiffness or histological fibrosis. Therefore, the models developed in this study should be interpreted as predicting risk groups based on the FIB-4 index rather than directly assessing histological fibrosis stage. Furthermore, potential misclassification, especially in the intermediate-risk group, should be considered. Second, this was a retrospective study conducted at a single institution. No external validation using an independent cohort was performed, and although four-fold cross-validation was applied, this approach does not establish generalizability. Therefore, multicenter validation is required before clinical translation. Third, the CT scanner used was a fast kV switching system; thus, further validation is required to determine whether these results can be applied to other types of dual-energy CT or scanners of different generations. Fourth, steatosis and iron accumulation, which could potentially influence MDI values, were not considered. Fifth, the heterogeneous etiologies of chronic liver disease included in the study population may have influenced the radiomic features. Finally, a moderate overlap between the intermediate-risk groups may have reduced discrimination performance.

CONCLUSION

The method employed in this study evaluated the predictive accuracy of FIB-4 index risk groups using CT, a noninvasive, and readily accessible modality. This study demonstrates the feasibility of combining dual-energy CT with radiomics for noninvasive liver fibrosis risk stratification using the FIB-4 index as a reference, warranting further validation.

Ethical approval: The research/study approved by the Institutional Research Ethics Committee at Hamamatsu University School of Medicine, number 22-169, dated December 08, 2022.

Declaration of patient consent: The Institutional Research Ethics Committee waived the requirement for informed consent. The authors declare that this study does not contain any personal information that could lead to patient identification.

Financial support and sponsorship: Nil.

Conflicts of interest: Takayuki Miyachi was previously employed by GE Healthcare.

Use of artificial intelligence (AI)-assisted technology for manuscript preparation: The authors confirm that there was no use of artificial intelligence (AI)-assisted technology for assisting in the writing or editing of the manuscript and no images were manipulated using AI.

REFERENCES

- Devarbhavi H, Asrani SK, Arab JB, Nartey YA, Pose E, Kamath PS. Global burden of liver disease: 2023 update. *J Hepatol* 2023;79:516-37.
- Roehlen N, Crouchet E, Baumert TF. Liver fibrosis: Mechanistic concepts and therapeutic perspectives. *Cells* 2020;9:875.
- Liedtke C, Nevzorova YA, Luedde T, Zimmermann H, Kroy D, Strnad P, *et al.* Liver fibrosis—from mechanisms of injury to modulation of disease. *Front Med (Lausanne)* 2022;8:814496.
- Battaller R, Brenner DA. Liver fibrosis. *J Clin Invest* 2005;115:209-18.
- Xiao G, Zhu S, Xiao X, Yan L, Yang J, Wu G. Comparison of laboratory tests, ultrasound, or magnetic resonance elastography to detect fibrosis in patients with nonalcoholic fatty liver disease: A meta-analysis. *Hepatology* 2017;66:1486-501.
- Zhang YN, Fowler KJ, Ozturk A, Potu CK, Louie AL, Montes V, *et al.* Liver fibrosis imaging: A clinical review of ultrasound and magnetic resonance elastography. *J Magn Reson Imaging* 2020;51:25-42.
- Park HC, Joo YS, Lee OJ, Lee K, Song TK, Choi C, *et al.* Automated classification of liver fibrosis stages using ultrasound imaging. *BMC Med Imaging* 2024;24:36.
- Ichikawa S, Goshima S. Clinical significance of liver MR imaging. *Magn Reson Med Sci* 2023;22:157-75.
- Watanabe H, Kanematsu M, Goshima S, Kondo H, Onozuka M, Moriyama N, *et al.* Staging hepatic fibrosis: Comparison of gadoxetate disodium-enhanced and diffusion-weighted MR imaging - preliminary observations. *Radiology* 2011;259:142-50.
- Ozaki K, Ohtani T, Ishida S, Higuchi S, Ishida T, Takahashi K, *et al.* Extracellular volume fraction obtained by dual-energy CT depicting the etiological differences of liver fibrosis. *Abdom Radiol (NY)* 2023;48:1975-86.
- Wang J, Tang S, Mao Y, Wu J, Xu S, Yue Q, *et al.* Radiomics analysis of contrast-enhanced CT for staging liver fibrosis: An update for image biomarker. *Hepatol Int* 2022;16:627-39.
- Noda Y, Goshima S, Nakashima Y, Miyoshi T, Kawai N, Kambadakone A, *et al.* Iodine dose optimization in portal venous phase virtual monochromatic images of the abdomen: Prospective study on rapid kVp switching dual energy CT. *Eur J Radiol* 2020;122:108746.
- Pfeiffer D, Parakh A, Patino M, Kambadakone A, Rummeny EJ, Sahani DV. Iodine material density images in dual-energy CT: Quantification of contrast uptake and washout in HCC. *Abdom Radiol (NY)* 2018;43:3317-23.
- Hertel A, Kuru M, Tollens F, Tharmaseelan H, Nörenberg D, Rathmann N, *et al.* Comparison of diagnostic accuracy of radiomics parameter maps and standard reconstruction for the detection of liver lesions in computed tomography. *Front Oncol* 2024;14:1444115.
- Gillies RJ, Kinahan PE, Hricak H. Radiomics: Images are more than pictures, they are data. *Radiology* 2016;278:563-77.
- Shah AG, Lydecker A, Murray K, Tetri BN, Contos MJ, Sanyal AJ, *et al.* Comparison of noninvasive markers of fibrosis in patients with nonalcoholic fatty liver disease. *Clin Gastroenterol Hepatol* 2009;7:1104-12.
- Fedorov A, Beichel R, Kalpathy-Cramer J, Finet J, Fillion-Robin JC, Pujol S, *et al.* 3D Slicer as an image computing platform for the quantitative imaging network. *Magn Reson Imaging* 2012;30:1323-41.
- Koo TK, Li MY. A guideline of selecting and reporting intraclass correlation coefficients for reliability research. *J Chiropr Med* 2016;15:155-63.
- Matsumoto K, Jinzaki M, Tanami Y, Ueno A, Yamada M, Kuribayashi S. Virtual monochromatic spectral imaging with fast kilovoltage switching: Improved image quality as compared with that obtained with conventional 120-kVp CT. *Radiology* 2011;259:257-62.
- Nahm FS. Receiver operating characteristic curve: Overview and practical use for clinicians. *Korean J Anesthesiol* 2022;75:25-36.
- Albrecht MH, Vogl TJ, Martin SS, Nance JW, Duguay TM, Wichmann JL, *et al.* Review of clinical applications for virtual monoenergetic dual-energy CT. *Radiology* 2019;293:260-71.
- Sofue K, Tsurusaki M, Mileto A, Hyodo T, Sasaki K, Nishii T, *et al.* Dual-energy computed tomography for noninvasive staging of liver fibrosis: Accuracy of iodine density measurements from contrast-enhanced data. *Hepatol Res* 2018;48:1008-19.
- Liu X, Qu L, Xie Z, Zhao J, Shi Y, Song Z. Towards more precise automatic analysis: A systematic review of deep learning-based multi-organ segmentation. *Biomed Eng Online* 2024;23:52.
- Bandula S, Punwani S, Rosenberg WM, Jalan R, Hall AR, Dhillon A, *et al.* Equilibrium contrast-enhanced CT imaging to evaluate hepatic fibrosis: Initial validation by comparison with histopathologic sampling. *Radiology* 2015;275:136-43.
- Marri UK, Das P, Shalimar, Kalaivani M, Srivastava DN, Madhusudhan KS. Noninvasive staging of liver fibrosis using 5-minute delayed dual-energy CT: Comparison with US elastography and correlation with histologic findings. *Radiology* 2021;298:600-8.
- Cicero G, Mazziotti S, Silipigni S, Blandino A, Cantisani V, Pergolizzi S, *et al.* Dual-energy CT quantification of fractional extracellular space in cirrhotic patients: Comparison between early and delayed equilibrium phases and correlation with oesophageal varices. *Radiol Med* 2021;126:761-7.

How to cite this article: Miyachi T, Ichikawa S, Kobayashi T, Osugi A, Suzuki R, Kakuya M, *et al.* Integration of dual-energy computed tomography and radiomics to improve noninvasive assessment of liver fibrosis: A retrospective study. *J Clin Imaging Sci.* 2026;16:8. doi:10.25259/JCIS_255_2025